Review

Fundamental understanding and modeling of reactive sputtering processes

S. Berg*, T. Nyberg

The Angstrom Laboratory, Uppsala University, Box 534, 751 21 Uppsala, Sweden

Abstract

Reactive sputtering is a commonly used process to fabricate compound thin film coatings on a wide variety of different substrates. The industrial applications request high rate deposition processes. To meet this demand, it is necessary to have very good process control of such processes. The deposition rate is extremely sensitive to the supply of the reactive gas. A too low supply of the reactive gas will cause high rate metallic sputtering, but may give rise to an understoichiometric composition of the deposited film. A too high supply of the reactive gas will allow for stoichiometric composition of the deposited film, but will cause poisoning of the target surface, which may reduce the deposition rate significantly. This behaviour points out that there may exist optimum processing conditions where both high rate and stoichiometric film composition may be obtained.

The purpose of this article is to explain how different parameters affect the reactive sputtering process. A simple model for the reactive sputtering process is described. Based on this model, it is possible to predict the processing behaviour for many different ways of carrying out this process. It is also possible to use the results of the modeling work to scale processes from laboratory size to large industrial processes. The focus will be to obtain as simple a model that will still quite correctly describe most experimental findings. Despite some quite crude approximations, we believe that the model presented satisfies this criterion.
© 2004 Elsevier B.V. All rights reserved.

Contents

* Corresponding author.
   E-mail addresses: soren.berg@angstrom.uu.se (S. Berg), tomas.nyberg@angstrom.uu.se (T. Nyberg).

1. Introduction

Reactive sputtering for thin film coatings is used in numerous industrial applications. By simply adding a gas that reacts with the sputtered material, it is possible to form a wide variety of useful compound thin film coatings. At first sight, this may seem very simple. However, the reaction mechanisms between the sputtered material and the reactive gas may cause some processing stability problems. Combining a high deposition rate and true compound stoichiometry of the deposited film turn out to appear as contradicting desires. In many cases, the main reason for this complication is that as well as forming a compound of the deposited film, compound formation will also take place at the surface of the sputtering target (target poisoning). Normally, the sputtering yield of the compound material is substantial lower than the sputtering yield of the elemental target material. This causes the deposition rate to decrease as the supply of the reactive gas increases. The relationship between the film composition and supply of reactive gas is very non-linear. This is also the case for the deposition rate vs. the supply of the reactive gas. Therefore, reactive sputtering processes controlled by the supply of the reactive gas exhibit quite complex processing behaviour [1,2].

Fig. 1 shows a typical experimental processing curve for the sputter erosion rate vs. the supply of the reactive gas for a reactive sputtering process (carried out with constant target current during processing). The characteristic feature of this curve is that it exhibits a hysteresis effect. The deposition rate does not decrease and increase at the same value with the supply of the reactive gas. The separation width between the decrease and increase denotes the width of the hysteresis region.

A corresponding hysteresis effect is observed for the relationship between the partial pressure and the supply rate

of reactive gas. This is shown in Fig. 2. This figure clearly illustrates a difference in increasing and decreasing the supply of the reactive gas. During the increase sequence of the reactive gas supply, the partial pressure of the reactive gas remains at a very low level until reaching the upper limiting value of the hysteresis width. During a decrease of the supply of the reactive gas, the partial pressure remains significantly higher in the hysteresis region than during the increase of the gas. This points out that more gas is consumed for compound formation during the increase sequence. This may be understood by comparing the sputter erosion rate curve for the corresponding sequences. A higher sputter erosion rate needs more reactive gas to form compound coatings.

The hysteresis effect is one of the key problems in experimental reactive sputtering systems. In the following treatment, we will therefore demonstrate how the hysteresis is affected by different processing parameters. The goal is to better understand the influence of processing parameters on the overall behaviour of this process.
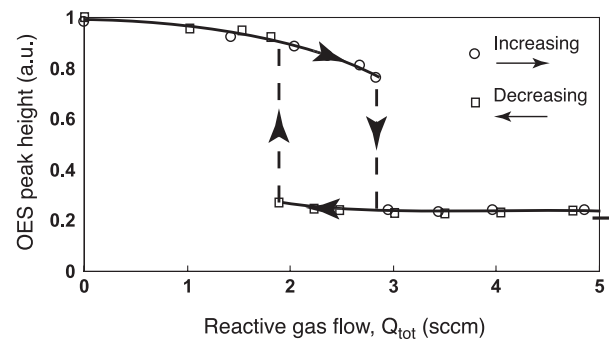

Fig. 1. Typical experimental curve for a reactive sputtering process. The optical emission (OES) from sputtered metal atoms represents the sputter erosion rate. Q_{tot} is expressed in standard cubic centimeters per minute (sccm).
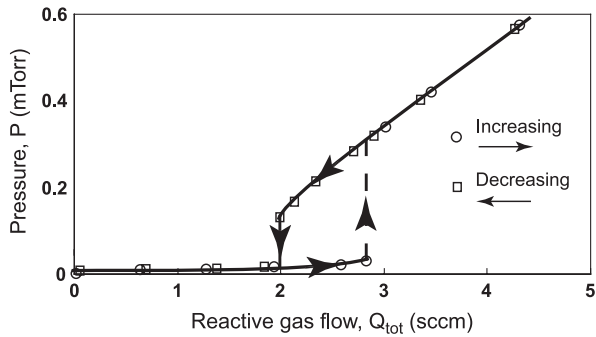
Fig. 2. The partial pressure, P, of the reactive gas corresponding to the curve in Fig. 1.

In order to be able to predict the outcome of reactive sputtering processes, there is a need for a reliable model. In the following paragraphs, we will outline a simple model for reactive sputtering processes. The core idea of this model has been published earlier [3]. It has become the commonly accepted treatment and is frequently referred to as "Berg's model". However, the results should be considered as first order approximations. Despite the simplicity, however, the results have proved to fit surprisingly well to most experimentally found results. There exist process conditions, however, where a more sophisticated treatment must be considered. Even in these cases, the treatment can be based on a similar balance philosophy as suggested in the basic simple "Berg's model" [3–8].

2. Definition of conditions for the reactive sputtering model

In order to understand the influence of different processing parameters for the reactive sputtering process, we will try to keep the number of parameters as low as possible. To satisfy this goal, we have as a first order approximation neglected some effects that may influence the overall processing behaviour. We will comment on this later in the article.

A schematic of a simple sputtering equipment is shown in Fig. 3. The mathematical model describing this system is
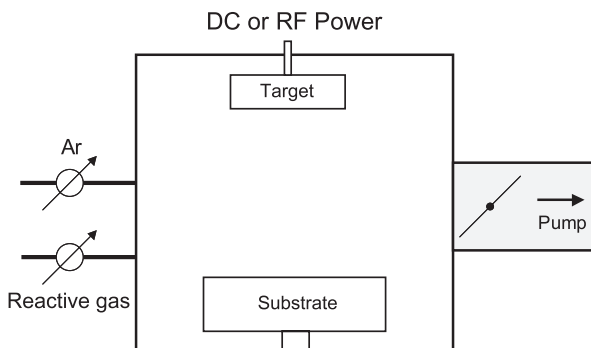

Fig. 3. Schematic of a simple reactive sputtering system.

shown in Fig. 4a–b. We assume a target (area A_t) in front of a collecting surface (area A_c) in a vacuum chamber. There is a pump connected to the vacuum chamber having a constant pumping speed S for the gases involved. A reactive gas supply is connected to the vacuum chamber. We assume that the following conditions exist in the chamber:

The total supply rate of the reactive gas is denoted Q_{tot}. There is a uniform partial pressure P of the reactive gas in the chamber. Since there is reactive gas present, the reactions between elemental target atoms and the reactive gas will cause a fraction θ_t of the target to consist of compound molecules. This compound formation is of course uniformly distributed over the whole target surface. To clearly illustrate that a fraction θ_t of the target has a different composition than the remaining $(1-\theta_t)$ fraction, we treat the θ_t fraction as a separate continuous area. The remaining part $(1-\theta_t)$ of the target surface consists of elemental non-reacted target atoms.

The same situation exists at the receiving area A_c where all sputtered material is assumed to be uniformly collected. The compound fraction at this surface area (deposited film) is denoted θ_c. Notice that, with this definition, θ_c is also a
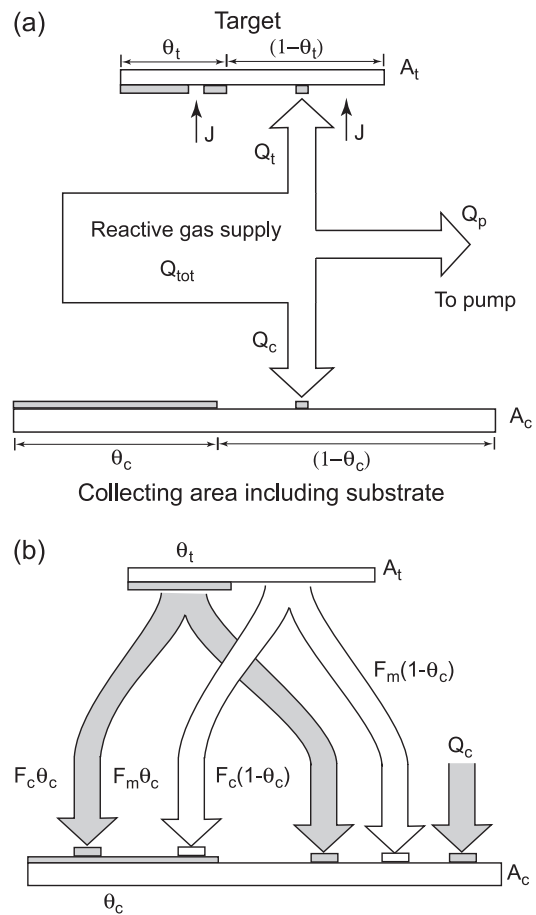

Fig. 4. (a) Theoretical equivalent for the system shown in Fig. 3. The notations are referred to and explained in the text. (b) Illustration of flux of sputtered material to the substrate area A_c. The notations are referred to and explained in the text.

measure of the composition of the deposited film. We also assume that the ratio between the electron and ion currents does not change during processing. The ion current density J (Amps/unit area) is assumed to be uniformly distributed over the target surface A_t. The sputtering contribution by ionized reactive gas is neglected, which is valid when the partial pressure of the reactive gas is significantly lower than the partial pressure of the argon gas. We also assume that sputtering of a compound molecule from the target surface results in exposing the original non-reacted surface at that target position. This corresponds to forming only one monolayer of the compound by chemisorption.

2.1. Flux of reactive gas in processing chamber

A uniform partial pressure P of the reactive gas will cause a uniform bombardment of neutral reactive molecules F (molecules/unit area and time) to all surfaces in the processing chamber. From gas kinetics [9], the relationship between F and P is

$$F = \frac{P}{\sqrt{2kT\pi m}}, \tag{1}$$

where k is the Boltzmann constant, T is the temperature and m is the mass of the gas molecule. In the following, we will derive steady-state values for some representative parameters during different processing conditions. The definition for steady state is that there be no time variations in the processing parameters. The consequences will be discussed in the following sections.

2.2. Conditions at the target surface

For simplicity, we assume the compound molecules at the target and substrate to consist of one reactive gas atom and one metal atom. Proper correction factors should be added for other stoichiometries. In the following description, we refer to Fig. 4a. During processing, the target will be sputter eroded. Elemental metal atoms are sputtered from the surface fraction $(1-\theta_t)$ and, for simplicity, the sputtered material from the surface fraction θ_t is assumed to be sputtered as molecules, irrespective of whether the material is ejected in atomic or molecular form. The only way sputtered compound molecules may be replaced is by reactions between neutral reactive gas molecules and the elemental non-reacted target material. We assume that no reactions between underlying elemental target atoms and the reactive gas can take place on the compound fraction θ_t of the target area A_t. A steady-state equation for the target may therefore be defined as

$$\frac{J}{q} Y_c \theta_t = \alpha 2F(1-\theta_t), \tag{2}$$

where Y_c is the sputtering yield of compound molecules from the compound-covered fraction θ_t of the target, α is the

probability (sticking coefficient) for a colliding neutral reactive gas molecule to react with an unreacted elemental target atom at the $(1-\theta_t)$ fraction of the target, q is the elementary electronic charge and F is multiplied by a factor of 2 because we assume two atoms per gas molecule. This equation states that at steady state the sputter erosion rate of compound molecules from the target must be identical to the compound formation rate by reactions between neutral reactive gas molecules and elemental target atoms. To further illustrate this, we have inserted a small compound area in front of the arrow corresponding to the incoming flux of reactive gas, Q_t, to the target surface. This symbolizes the rate of compound formation at the target. We have also "opened up" a small hole in the θ_t fraction area of the target. This is to illustrate the sputter removal rate of the compound material from the target. At steady state, the compound area to the right must "replace" the hole to the left. From Eqs. (1) and (2), it is possible to solve for θ_t as a function of partial pressure of the reactive gas.

2.3. Conditions at collecting area (substrate)

We assume that all sputtered material from the target will be uniformly deposited at the collecting area A_c. At steady state, the composition of added film material must be identical to the existing film composition. There are several ways of describing this situation.

2.3.1. Flux of material approach

By the following arguments, θ_c may be evaluated. The descriptions refer to Fig. 4b. The total number of out-sputtered compound molecules per unit time from the target will be denoted F_c.

$$F_c = \frac{J}{q} Y_c \theta_t A_t, \tag{3a}$$

where Y_c represents the sputtering yield of the compound material. We assume that this compound material will be uniformly distributed onto the collecting surface A_c. Notice, however, that $(F_c\theta_c)$ will be deposited at the fraction θ_c of A_c that already has been defined to consist of compound material. Adding compound material to the already existing compound fraction of the collecting area will not change the local composition. Consequently, the addition of $(F_c\theta_c)$ to the θ_c fraction at the collecting area A_c will not influence the surface fraction θ_c. This contribution will therefore be neglected in this treatment.

The remaining fraction $F_c(1-\theta_c)$ of sputtered compound material will be deposited onto the fraction $(1-\theta_c)$ of the collecting area A_c containing elemental non-reacted target atoms. This will convert some part of the $(1-\theta_c)A_c$ area to become part of the θ_c fraction of compound material at the surface A_c. This fraction of the deposited compound material will thus contribute to an increase in the value of θ_c.

2.3.2. Sputtered elemental target atoms

A corresponding argument may be applied to the sputtered non-reacted elemental target atoms, for which the total number per unit time in Fig. 4b is denoted by

$$F_m = \frac{J}{q} Y_m (1 - \theta_t) A_t \tag{3b}$$

The fraction of flux $F_m(1-\theta_c)$ deposited onto the fraction $(1-\theta_c)$ of the collecting area A_c will not influence the value of θ_c. Adding elemental non-reacted target atoms to an area already defined to consist of non-reacted atoms does not change θ_c. However, the flux $F_m\theta_c$ deposited onto the fraction θ_c of compound material at the collecting area A_c will contribute to a decrease in θ_c.

Compound formation by reaction between reactive gas molecules and elemental non-reacted atoms at the collecting area will consume Q_c reactive gas molecules. As for the target, we assume that no reactions between elemental target atoms and the reactive gas can take place on the compound fraction θ_c of the collecting area. Therefore,

$$Q_c = \alpha F (1 - \theta_c) A_c. \tag{3c}$$

For simplicity, we assume the same value for α as for the target. Since the reactive gas molecules consist of two atoms, Q_c will contribute with two compound molecules adding to the value of θ_c. At steady state, the contributions supporting an increase in θ_c must be identical to the contributions that support a decrease in θ_c. This leads to the following balance equation for the collecting area A_c,

$$2Q_c + F_c (1 - \theta_c) = \theta_c F_m. \tag{3}$$

From Eqs. (1)–(3), it is possible to solve for θ_c as a function of the partial pressure of the reactive gas.

2.3.3. Material conservation approach

Some arguments have been raised against the above approach; namely, that the flux of materials approach described in Sections 2.3.1 and 2.3.2) above neglects some of the outsputtered material ($F_c\theta_c$) and $F_m(1-\theta_c)$. The following alternative treatment, however, serves to support the validity of the balance treatment.

The ratio $\theta_c/(1-\theta_c)$ between the compound and elemental target atom fractions in the deposited film must be identical to the corresponding ratio $(F_c+2Q_c)/F_m$ of the added film material. This relation defines a balance equation for the collecting area A_c,

$$\frac{\theta_c}{1 - \theta_c} = \frac{F_c + 2Q_c}{F_m} \tag{3'}$$

By solving Eqs. (3) and (3') for θ_c, we find that both these equations result in identical expressions for θ_c. The "flux of material" and "material conservation" approaches give rise to identical mathematical conditions for the steady-state conditions at the collecting area A_c.

2.4. Deposition rate

Using the above notation, it is easy to define an expression for the total sputter erosion rate R from the target (atoms+molecules per unit area and time),

$$R = \frac{J}{q} [Y_m (1 - \theta_t) + Y_c \theta_t]. \tag{4}$$

Proper constants may be added to convert R into desired units (e.g., angstrom/min, etc.). It must be understood, however, that more material is deposited at the collecting area A_c than sputter eroded from the target area A_t. This is because Q_c of the reactive gas is added to the sputtered flux of material. The difference in mass between sputter eroded material and the mass of the deposited material will strongly depend on the content of reactive gas atoms in the compound molecule per sputtered elemental metal atom. An expression for the deposition rate D may be obtained in the following way. The total sputtering rate R_m of metal atoms (elemental+those included in sputtered molecules) is

$$R_m = \frac{J}{q} [Y_m (1 - \theta_t) + Y_c \theta_t] A_t. \tag{5'}$$

Knowing the compound fraction θ_c at A_c makes it quite easy to derive an expression for the deposition rate D.

$$D = c_1 R_m (1 - \theta_c) + c_2 R_m \theta_c, \tag{5}$$

where c_1 and c_2 are constants accounting for unit conversions. The first term in Eq. (5) represents the contribution by elemental metal atoms, while the second term represents the contribution by compound material. We have chosen to express normalized D in units of mass/unit time.

2.5. Modeling as a function of reactive gas partial pressure P

From Eqs. (1)–(5), it is possible to calculate R, D, θ_t and θ_c as a function of partial pressure P. Typical curves are shown in Figs. 5 and 6). Numerical values used for the calculations are given in Appendix Notice that all curves
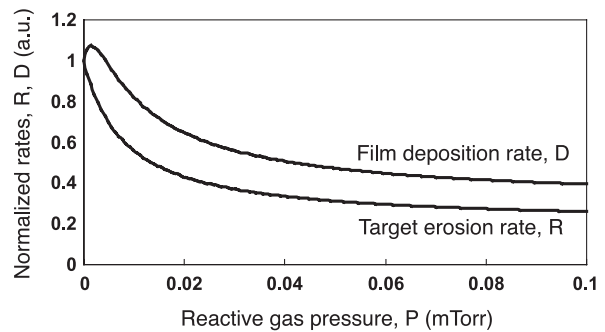

Fig. 5. Calculated target erosion rate R and substrate deposition rate D vs. partial pressure, P, of the reactive gas.
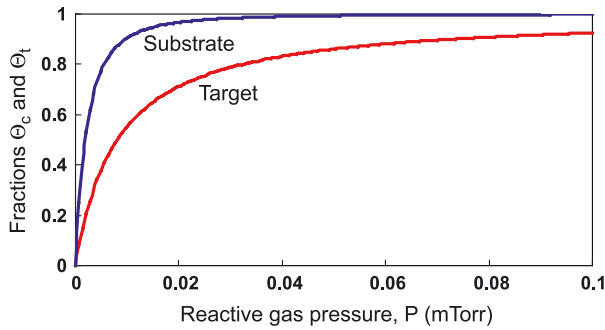
Fig. 6. Calculated compound fractions θ_t and θ_c at the target and substrate, respectively, as a function of the partial pressure, P, of the reactive gas.
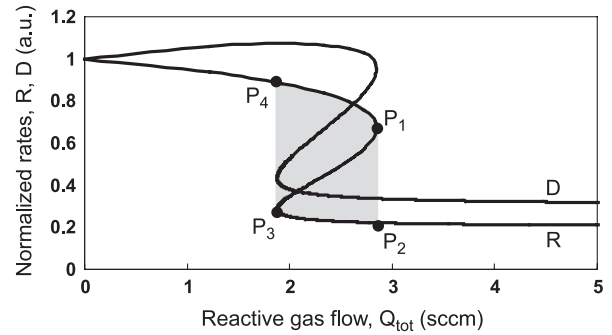

Fig. 7. Calculated target erosion rate R and substrate deposition rate D vs. total supply rate of reactive gas, Q_{tot}, for conditions identical to those used in generating Figs. 5 and 6.

are "well behaved" and give single valued results at all partial pressures. Moreover, the deposition rate curve may have a maximum value before reaching complete target poisoning. These curves correspond to the reactive deposition of AlN.

Unfortunately, it is not easy to experimentally control the partial pressure of the reactive gas during processing. Therefore, simple processing curves like Figs. 5 and 6 will not be obtained without quite sophisticated process control systems. The simplest and most common control function is the supply of reactive gas to the processing chamber. This calls for modeling equations based on the supply of the reactive gas rather than based on the partial pressure.

2.6. Kinetics of the reactive gas

The relation between the reactive gas supply and the partial pressure may quite easily be solved from the model outlined above where the compound formation (reactions between elemental target atoms and reactive gas molecules) consumes a fraction of the incoming gas. A schematic diagram of the reactive gas pathways was shown in Fig. 4a. The consumption (number of molecules per unit time) at the target Q_t is obtained from Eq. (2),

$$Q_t = \alpha F(1 - \theta_t)A_t, \tag{6a}$$

while the consumption Q_c at the collecting area A_c is obtained from Eq. (3c).

$$Q_c = \alpha F(1 - \theta_c)A_c. \tag{6b}$$

The remaining part Q_p of the reactive gas will escape from the processing chamber through the pumping system. Assuming a pumping speed of S for the system pump gives

$$Q_p = SP. \tag{6c}$$

The total supply Q_{tot} is the sum of all sources for reactive gas consumption,

$$Q_{tot} = Q_t + Q_c + Q_p. \tag{6}$$

2.7. Modeling as a function of the total reactive gas supply rate Q_{tot}

Adding Eq. (6) to the previous equations makes it possible to find the relation between Q_{tot} and P, and consequently calculate R, D, θ_t, θ_c, Q_t, Q_c, Q_p and P as a function of the supply rate of the reactive gas Q_{tot}. Results are shown in Figs. 7–9. It is obvious that these curves show a more complex relation to Q_{tot} than the curves in Figs. 5 and 6 did to the partial pressure P. The S-shaped behaviour defines a region where one value for Q_{tot} may be satisfied by three different values of R, D, P, θ_t and θ_c. This region corresponds to the hysteresis width shown in Figs. 1 and 2 in the introduction. Four different points, P_1–P_4, are marked in Figs. 7–9. In the following, we discuss important phenomena that take place at these positions. Before elaborating on this, however, we clarify two different modes of operation.

It is important to understand the difference between processes controlled by partial pressure of the reactive gas and by the supply of the reactive gas. This difference is illustrated in Fig. 10a–b. Selecting values for the partial pressure in Fig. 10a corresponding to positions 1, 2, ..., 9 on the curve result in well-defined single-valued supply levels Q_{tot}. Thus, by selecting continuously increasing
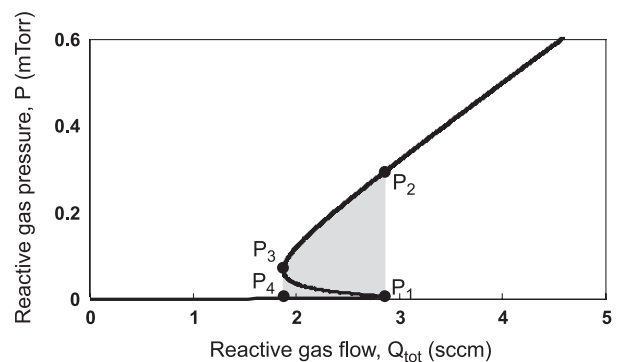

Fig. 8. Calculated partial pressure, P, vs. supply rate of the reactive gas, Q_{tot}.
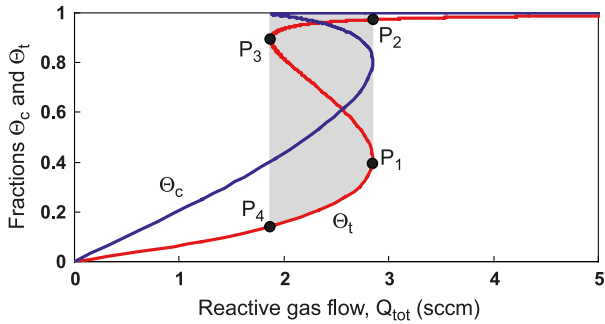
Fig. 9. Calculated compound fractions θ_t and θ_c for the target and substrate, respectively, vs. supply of the reactive gas, Q_{tot}. P_1–P_4 are only marked for the θ_t-curve.

values of the partial pressure of the reactive gas, the S-shaped curve shown in Fig. 10a will be generated. This is the signature of a partial pressure process control.

As previously shown in Fig. 5 in Section 2.5, any selected partial pressure value also corresponds to a well-defined single value of the sputter erosion rate R. Thus, it is possible to obtain paired values (R, Q_{tot}) corresponding to specifically selected partial pressures. These (R, Q_{tot}) pair values will define a R vs. Q_{tot} curve with the shape shown in Fig. 10b. It must be understood that experimentally this curve can only be generated by stepping values of the partial pressure not by stepping values of the reactive gas supply. In practice, this curve can only be obtained for processes having some feedback control system enabling, in a controlled way, variations in the reactive gas supply corresponding to the desired values of the partial pressure.

A different behaviour will result if the supply rate of the reactive gas Q_{tot} is used as the process control parameter. Continuously increasing Q_{tot} can not generate the entire S-shaped curve in Fig. 10b. When Q_{tot} reaches the value corresponding to position 2 on the curve, a dramatic effect occurs. A small additional increase in Q_{tot} forces the rate to avalanche from position 2 down to position 7 on the curve. An even further increase of Q_{tot} generates R values 8, 9, etc., following the curve.

Starting at high gas flow values (corresponding to position 9 on the curve) and then decreasing Q_{tot} generates values of the erosion rate R following the curve in reverse order to position 4. However, at this point, a further decrease in Q_{tot} will result in R avalanching from position 4 to a point somewhat to the left of position 1. A further decrease in Q_{tot} will cause the rate R to follow the curve. The fact that the sharp decrease and increase of R do not occur at the same value for Q_{tot} illustrates the hysteresis effect with the hysteresis width defined by the separation between the two avalanche positions. This is the way that the R responds experimentally to having the supply Q_{tot} as the input control parameter. It must also be pointed out that, in this mode of operation, it is not possible to reach any of the processing points on the segment between the positions 2 and 4 on the curve. Instead of following the S-shaped loop on this

segment, the process will by-pass the loop and avalanche along the dotted lines.

Thus, the positions labeled P_1–P_4 in Figs. 7–9 denote the processing region (shown shadowed) in which hysteresis occurs.

3. Parameters influencing the hysteresis effect

There exist many "popular" explanations regarding the origin of the hysteresis effect in reactive sputtering processes. A too simplified explanation, however, may cause the experimentalists to draw wrong conclusions concerning how to optimize the process. We therefore want to clarify parametric interactions in somewhat more detail. It should be pointed out that, although hysteresis is generally observed in reactive sputter processing, there also exists conditions under which hysteresis does not occur. It is possible to use the mathematical model outlined above to analyze specific processes and predict if hysteresis will appear or not.

In order to investigate the influence of processing parameters on the reactive sputtering process, we will introduce some illustrative curves. Plotting the curves for Q_{tot}, Q_t, Q_c and Q_p as a function of P may clarify the gettering situation. This is shown in Fig. 11a where it is clear that among the supply rate components, only Q_c exhibits a negative derivative dQ_c/dP in a limited section of the curve. Q_t and Q_p do not have negative derivatives. It is therefore the negative derivative portion of the Q_c curve that
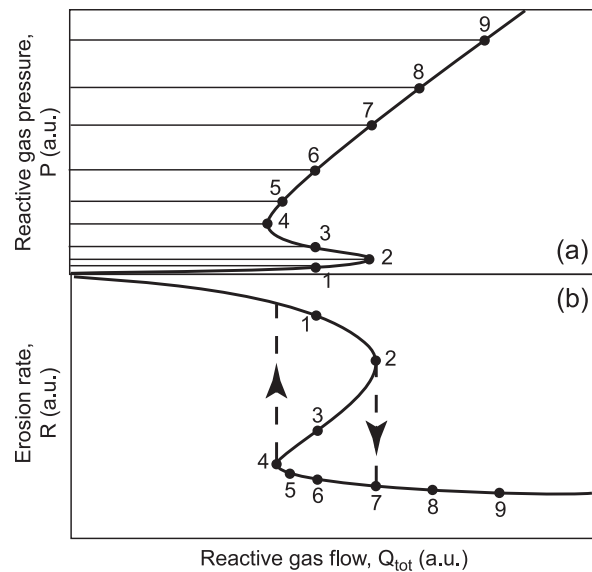

Fig. 10. Schematic diagram illustrating the simulation procedure. (a) shows the general behavior for the reactive gas pressure, P, vs. reactive gas flow and (b) shows sputtering rate, R, vs. reactive gas flow. By selecting different values for the partial pressure in (a), the process operates at different points indicated by 1, 2, ..., 9. These points correspond to points 1, 2, ..., 9 in (b).
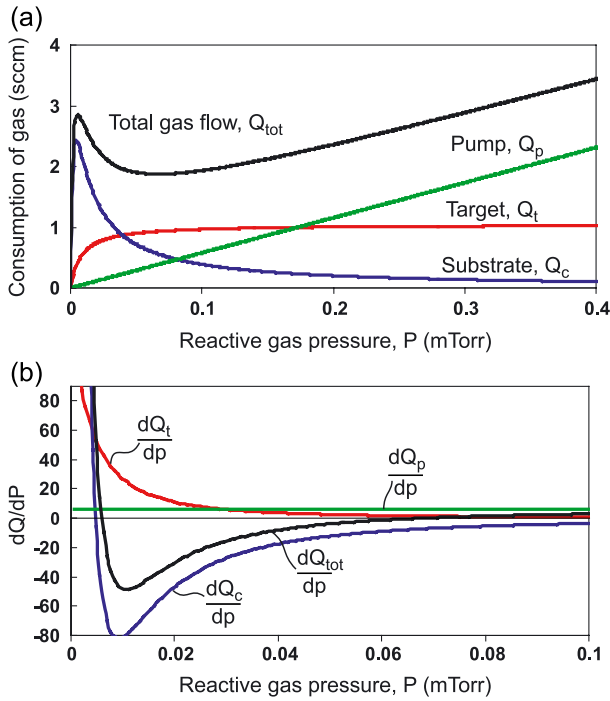
Fig. 11. (a) shows calculated consumptions of the reactive gas vs. the partial pressure of this gas and (b) shows calculated derivatives of the consumption curves shown in (a).

causes a negative derivative in the Q_{tot} vs. P curve. Having (or eliminating) hysteresis may be predicted by investigating the conditions for the derivative dQ_{tot}/dP. If $dQ_{tot}/dP<0$ in some region, the process will exhibit hysteresis. If $dQ_{tot}/dP>0$ over the whole processing region, then the process will not exhibit any hysteresis. In Fig. 11b are shown the derivatives of Q_{tot}, Q_c, Q_t and Q_p as a function of P. The following condition is valid,

$$\frac{dQ_{tot}}{dP} = \frac{dQ_t}{dP} + \frac{dQ_c}{dP} + \frac{dQ_p}{dP}. \qquad (7)$$

Eq. (7) is quite useful when determining whether hysteresis will appear or not. (Notice that $dQ_p/dP=S$, system pumping speed.)

The functions Q_t, Q_c and Q_p may also be presented as a function of Q_{tot}. Such a presentation is shown in Fig. 12.
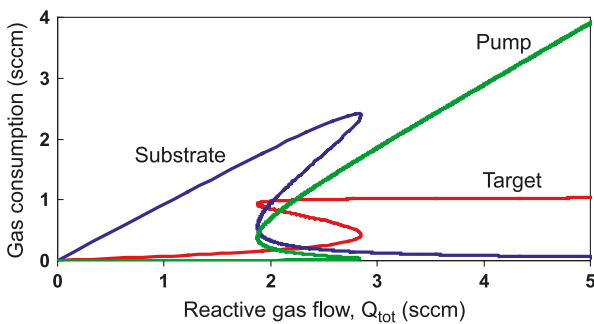

Fig. 12. Calculated consumption of the reactive gas vs. the supply, Q_{tot}, of this gas.

3.1. Influence of target material

The sputtering yields Y_m for the elemental target material and Y_c for the compound formed on the target surface are materials constants. For materials where $Y_c \ll Y_m$, hysteresis is normally more pronounced than if Y_c is close to Y_m [10].

In Fig. 13, three R vs. Q_{tot} curves calculated for different values of Y_c, keeping Y_m constant, are shown. As can be seen, there is a pronounced difference in hysteresis width for the curves. The model thus predicts that different target materials may respond differently in a reactive sputtering process.

3.2. Influence of reactive gas

Some gases are more reactive to the target material than others. Normally, O_2 is a more aggressive gas than N_2. The influence of gas reactivity may be simulated by changing the value of the sticking coefficient α in the model formulas. In Fig. 14, the results of R vs. Q_{tot} for different values of α are shown. Notice that a decrease in α causes a decrease in the width of the hysteresis region [11]. Also, α may be considered as a materials constant. However, this constant may be influenced by, e.g., target/substrate temperatures, surface morphology, etc.

3.3. Influence of system pumping speed

In many reactive sputtering processing chambers there is a throttle valve between the pump and the chamber. The setting of this valve determines the pumping speed for the external pump. It is thus possible to experimentally control the pumping speed. Fig. 15 shows the effect of varying the pumping speed. The calculations predict that the hysteresis may be eliminated if the pumping speed is high enough. This is a well known effect [12] and it can also be seen directly by inspection of Eq. (7) and Fig. 11a–b. Since $S=dQ_p/dP$, the value of S may always be chosen high enough to make $dQ_{tot}/dP>0$. Unfortunately, the critical value of the pumping speed needed to eliminate the hysteresis is usually unrealistically high.
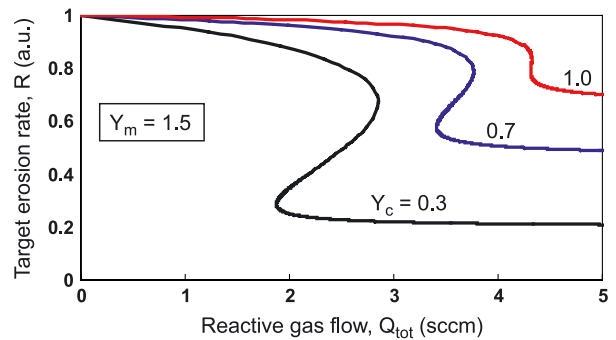

Fig. 13. Calculated sputter erosion rates, R, vs. the supply, Q_{tot}, of reactive gas for different values of the sputtering yield Y_c for the compound, $Y_m=1.5$.
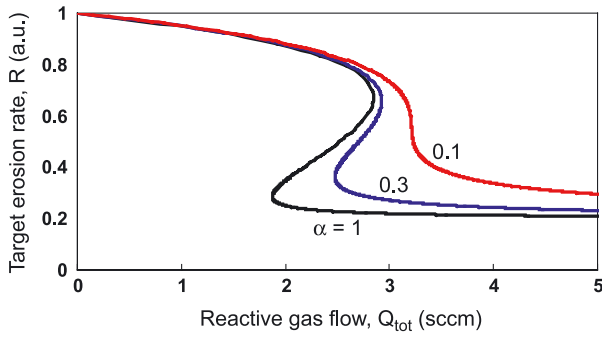
Fig. 14. Calculated sputter erosion rates, R, vs. reactive gas supply, Q_{tot}, for three different values of the sticking coefficient α.

3.4. Target to substrate distance

The position of the target in front of the substrate may also influence the hysteresis width. This is illustrated by changing the size of the collecting area A_c in the calculations. An increasing collecting area A_c represents an increasing target to substrate distance. Fig. 16 shows the processing curves for two different sizes of A_c. Keeping the target to substrate distance small will cause a decrease in the hysteresis width. Notice that there will always be some spread of the sputtered material. Therefore, the condition that $A_c > A_t$ will always exist in this configuration.

Many sputtering systems have shutters relatively close in front of the sputtering cathodes. It is common practice by many users to pre-sputter the target behind a shutter before exposing the substrate to film deposition. The idea is to obtain stable processing conditions before exposing the substrate to deposition. The use of a target shutter in reactive sputter deposition, however, may significantly influence the processing conditions. Pre-sputtering the target in reactive mode behind the shutter will be equivalent to sputtering with a smaller collecting area than the collecting area when the shutter is removed. The reactive sputtering process will then "jump" from one processing curve corresponding to the shutter area to another corresponding to the deposited area when the shutter is removed (illustrated by the arrow in Fig. 16). After the shutter removal, a new stabilization period will take place before reaching the new steady-state
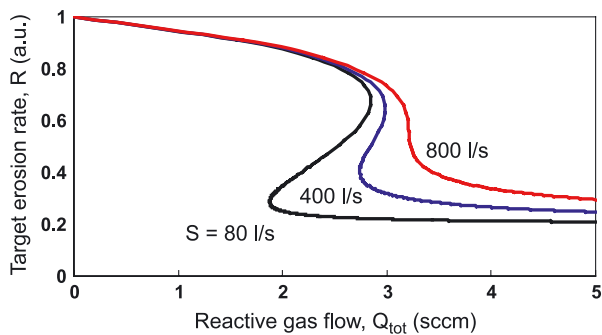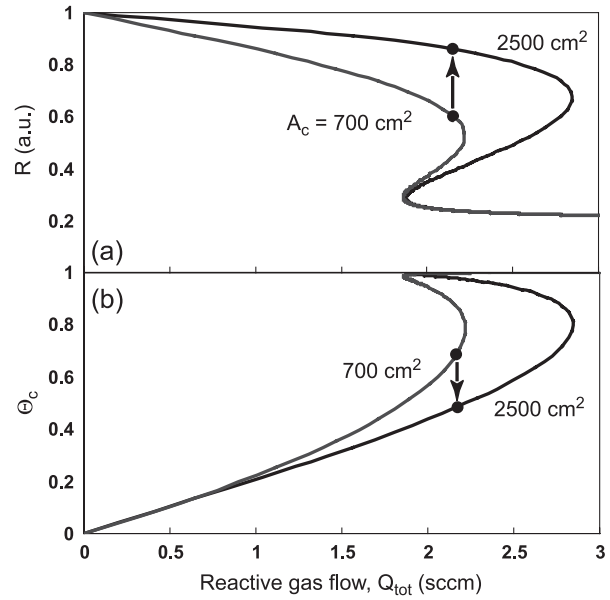

Fig. 16. Calculated processing curves corresponding to sputtering with a target shutter (A_c=700 cm^2) and without a shutter (A_c=2500 cm^2).

condition. During this period, the composition of the deposited film may vary significantly. This initial phase of deposition determines the film/substrate interface. This may affect the film adhesion and other film/substrate sensitive properties.

However, having a protective shutter close to the substrate instead of close to the target will make it possible to pre-sputter in reactive mode without any significant change in mode of operation when the shutter is removed (minor change in A_c).

3.5. Target ion current

At first, it might seem possible to eliminate the hysteresis by applying high power to the target and thus reducing the target poisoning effect by a high sputter erosion rate. Unfortunately, the process does not respond in this way. In Fig. 17, results of calculations for different ion current levels are shown. Increasing the ion current only causes a magnification of the curves. In fact, the calculations predict

Fig. 15. Calculated sputter erosion rates, R, vs. reactive gas supply, Q_{tot}, for three different pumping speeds, S.
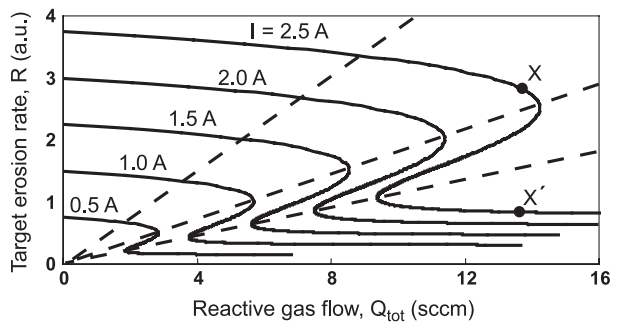

Fig. 17. Calculated sputter erosion rates, R, vs. reactive gas supply, Q_{tot}, for different values of the argon ion current, I. Dashed lines represent constant compositions θ_t and θ_c.

that the target poisoning and the film composition effects will be identical along straight lines starting from the origin. It is thus not possible to eliminate the hysteresis by increasing the target ion current.

The hysteresis effect may also cause confusion in decisions concerning the processing point. It is often desired to operate the process close to the avalanche point. A suitable operating point for the I=2.5 A curve in Fig. 17 should be point X. This point may be reached by first applying 2.5 A to the target and then slowly increasing Q_{tot} to $\approx$ 13 sccm. Note, however, that, if 13 sccm of reactive gas is supplied to the processing chamber before the target current is applied, the process will end up at processing point X'. Identical sets of values for Q_{tot} and I yield different processing conditions. This serves to illustrate that under certain conditions it is important to report in which order different parameters are applied to the process.

Sometimes, the target current or power supplied to the target may be used as a control processing parameter. If a constant supply of reactive gas is fed to the chamber, this will give the curves in Fig. 18a–b for the sputter erosion rate R and partial pressure P as a function of target ion current.

Notice that, for low values of the ion current, the target is poisoned, while the metallic target mode corresponds to high values of ion current. This same information can also be obtained from Fig. 17.

3.6. Target area: hysteresis-free operation

It is possible to select the size of the target. The model predicts that the shape of the processing curves depend strongly on the size of the "effective" target area. This is shown in Fig. 19a. As can be seen, there will be no hysteresis for a small size target area under these processing conditions
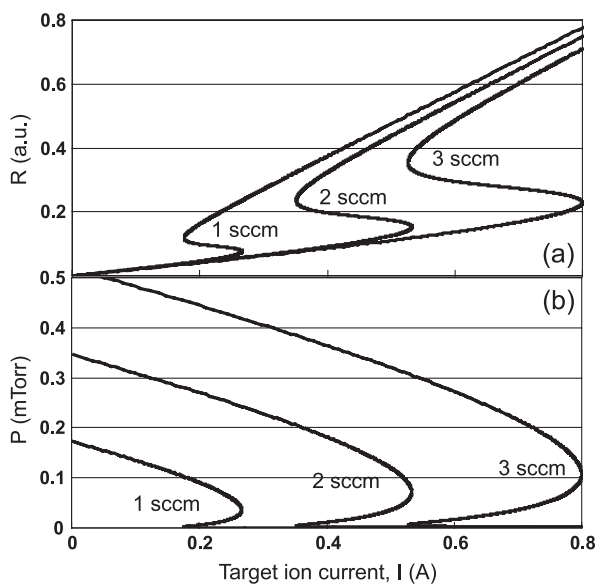

Fig. 18. Calculated processing curves using ion current, I, as the independent parameter. (a) Target erosion rates, R. (b) Partial pressure of reactive gas, P.
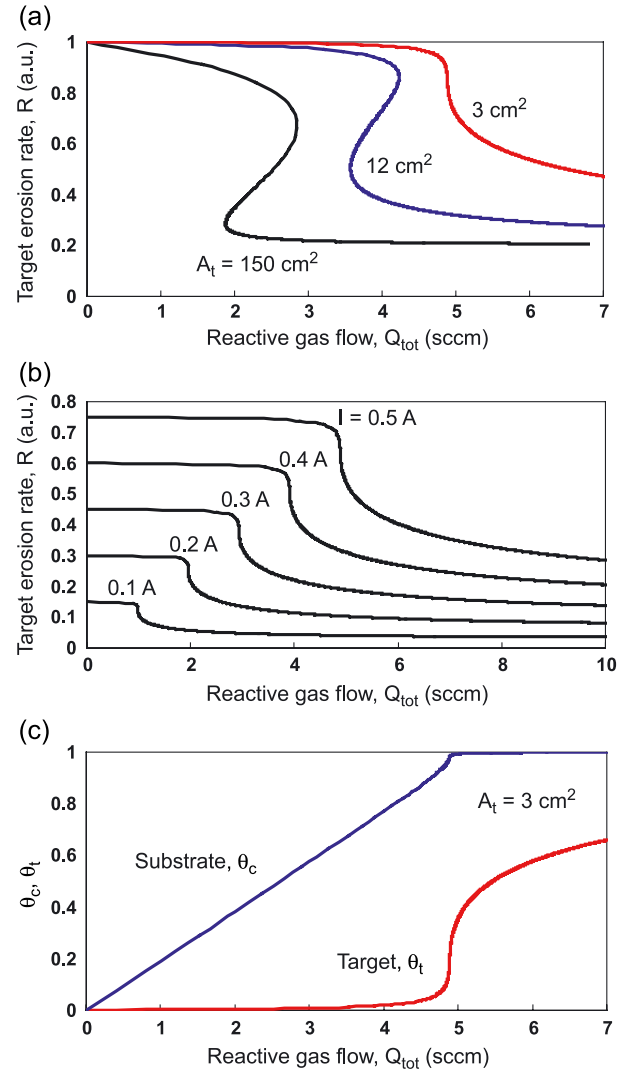

Fig. 19. (a) Calculated sputter erosion rates, R, vs. reactive gas supply, Q_{tot}, for different values of the target area, A_t, assuming a constant total target ion current, I. (b) Calculated sputter erosion rates, R, vs. reactive gas supply, Q_{tot}, for different values of target ion current, I, for the 3-cm^2 target in (a). (c) Calculated values for θ_t and θ_c vs. reactive gas supply, Q_{tot}, for the 3-cm^2 target in (a).

[13]. It must be pointed out that this is not an effect caused by the corresponding increase in ion current density (having the same total target current for all target areas). To further illustrate this, calculations for the small area target for different target ion currents are shown in Fig. 19b. As can be seen, the hysteresis is eliminated irrespective of ion current density values. This is a consequence of the results described in Fig. 17. Increasing or decreasing the ion current only causes a magnification or demagnification of the curves. It does not change the shape of the curves.

A small target exhibits almost ideal processing conditions. Fig. 19c shows the compound fractions θ_t and θ_c corresponding to the same conditions as in Fig. 19a for A_t=3 cm^2. Note that the target remains primarily in the high rate metallic mode $\theta_t \approx 0$ all the way up to the position where $\theta_c \approx 1$ (stoichiometric film formation).

It should be noticed, however, that the critical target size for hysteresis-free operation will depend on several other processing parameters. The critical size has to be estimated for the specific reactive sputtering process. Notice also that the power dissipation over a relatively small area may give rise to a considerable heating of the target. This has to be considered when designing a hysteresis-free reactive sputtering process based on this phenomenon.

4. Dissociation of sputtered compound molecules: effect on modelling

In the above treatment, we assumed that the sputtered compound molecules from the target reached the collecting area without breaking up into free atoms [14]. This is generally not believed to occur for compound molecules during sputtering. During the sputter event, the compound molecule is believed to dissociate into its elemental atoms. It is easy, however, to modify the above model to take molecule dissociation into account. This may be illustrated by the following arguments.

(a) In the case of compound dissociation, there will be no net gettering of the reactive gas at the target surface. The reason for this is that the gas molecules that are consumed to form the compound at the target surface will return to the gas when the compound molecule is sputtered and dissociated into its original components. We simply assume that these "gas atoms" will return back to the gas phase.

(b) There will be an additional flux of elemental target atoms to the collecting area A_c. Compound molecules will be sputter eroded from the target at a rate $(J/q)Y_c\theta_c$. The metal fraction of these outsputtered compound molecules will, after compound dissociation, reach the collecting area as elemental target metal atoms.

In Fig. 20, results from calculations based on the dissociation of the compound molecules are compared to
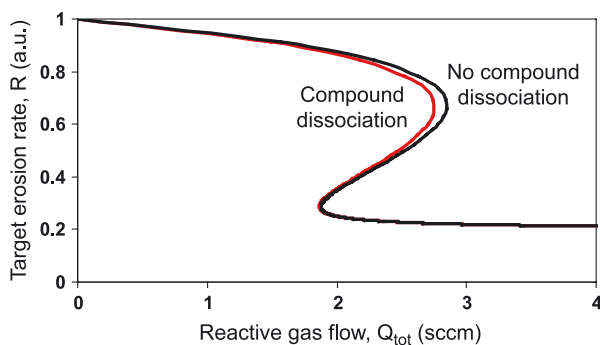

Fig. 20. Calculated sputter erosion rates, R, vs. reactive gas supply, Q_{tot}, including the effect of molecular dissociation and neglecting this effect.

the results based on sputtered compound molecules. It is observed that there is only a minor difference between the two curves. Detailed comparisons of θ_t, θ_c, Q_c, Q_t and P as a function of Q_{tot} give the same minor deviations as for the R vs. Q_{tot} curve shown in this figure. This illustrates that the status of the sputtered material does not primarily determine the general shapes of these curves. Other parameters have a far more significant influence on the overall process. In the following treatments, we therefore choose to continue to allow sputtered compound molecules to reach the substrate intact.

5. Reactive co-sputtering

Complex compound thin films may be deposited by reactive co-sputtering from several elemental targets [15]. The processing behaviour for such a set-up can be predicted by calculations based on the simple model presented above. It is necessary, however, to somewhat modify the conditions at the collecting area compared to that outlined for a single elemental target. We suggest the following treatment.

A schematic of the model for the processing situation for a reactive co-sputtering process having two separate targets is shown in Fig. 21. The notation corresponds to the definitions given in Fig. 4a–b. Eq. (2) may be used to define the balances for each separate target.

$$\frac{J_1}{q} Y_{c1}\theta_{t1} = \alpha_1 2F(1 - \theta_{t1}) \tag{8a}$$

for target 1 and

$$\frac{J_2}{q} Y_{c2}\theta_{t2} = \alpha_2 2F(1 - \theta_{t2}) \tag{8b}$$

for target 2.

The conditions at the collecting area A_c are somewhat more complicated than for the simple single target process. We choose to use the material conservation approach (Eq. (3′)) to solve for the overall composition y of the collecting area A_c. The total number T_1 of sputtered elemental atoms from target 1 is given by

$$T_1 = \frac{J_1}{q} A_1 [Y_{m1}(1 - \theta_{t1}) + Y_{c1}\theta_{t1}], \tag{9a}$$

assuming one metal and one gas atom in the compound molecule. A corresponding equation may be defined for the second target,

$$T_2 = \frac{J_2}{q} A_2 [Y_{m2}(1 - \theta_{t2}) + Y_{c2}\theta_{t2}]. \tag{9b}$$

From T_1 and T_2, the fraction y of metal 1 atoms in the deposited film may be calculated as
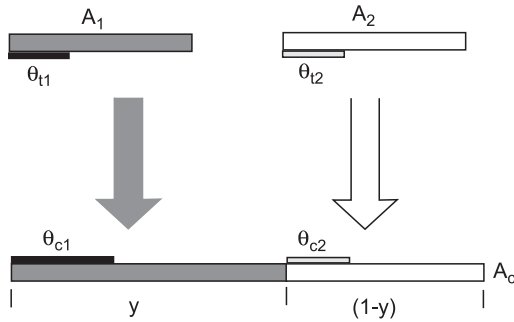
$$y = \frac{T_1}{T_1 + T_2}. \tag{9}$$

Fig. 21. Schematic diagram of a reactive co-sputtering system having two targets.

Fig. 23. Calculated fraction, y, of material 1 in mixed deposited film vs. reactive gas supply, Q_{tot}, for reactive co-sputtering (solid line) and reactive alloy sputtering (dashed line).

These equations may then be used to calculate the compound fractions θ_{c1} and θ_{c2} at the surface fractions yA_c and $(1-y)A_c$ of the collecting area. Since y was defined to be the fraction of atoms sputtered from target 1, we simply assume that all material sputtered from target 1 is collected at the y fraction of A_c. Therefore, collecting of materials from the two separate targets may be treated separately.

A relationship between the partial pressure and supply of the reactive gas can be found that is analogous to the treatment for one gas and one target. Notice, however, that all sub-areas $A_{t1}(1-\theta_{t1})$, $A_{t2}(1-\theta_{t2})$, $yA_c(1-\theta_{c1})$ and $A_c(1-y)(1-\theta_{c2})$ consume reactive gas.

Calculations based on the assumptions made here are shown in Fig. 22. We have chosen processing conditions to demonstrate that the width and position of the hysteresis obtained by simultaneous sputtering of both targets (co-sputtering) may deviate significantly from operating any of the targets individually. Notice also that we only obtain a single hysteresis and not a complex mixture of two hystereses.

Due to the different reactivity of the two targets, and also the different ratios Y_c/Y_m of the targets, the film composition y may vary quite dramatically as a function of the reactive gas supply Q_{tot}. In Fig. 23, the composition y as a function of reactive gas supply is shown for the co-sputtering curve shown in Fig. 22. The loop illustrates that quite complex composition behaviour may be obtained for reactive co-
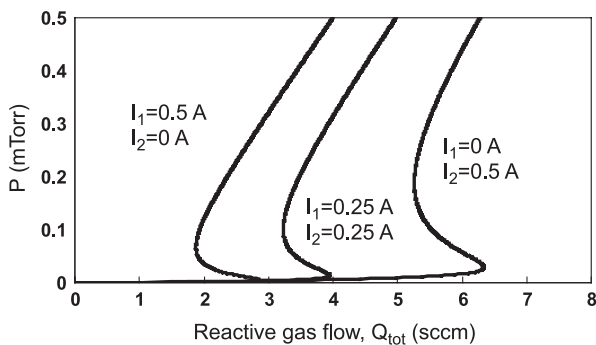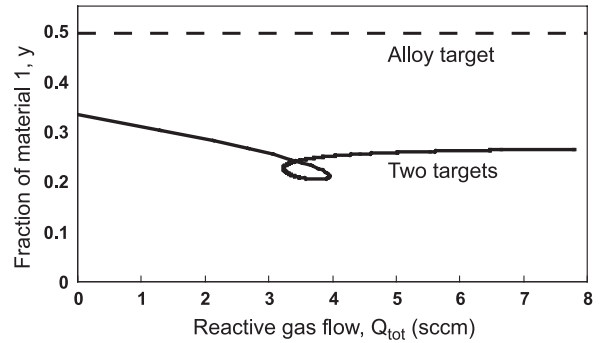

Fig. 22. Calculated partial pressures, P, vs. supply, Q_{tot}, of the reactive gas for the cases in which the targets are operating individually or both are operating simultaneously.

sputtering from two separate targets. Increasing the number of targets further increases the complexity.

We also want to point out that due to different reactivities between targets and the reactive gas, it may be impossible to operate both targets in the metallic mode (high rate sputtering) and obtain a fully reacted coating. However, this can only be achieved for certain specific compositions. This effect will exist for both reactive alloy and co-sputtering.

6. Reactive sputtering from an alloy target

Due to the materials conservation, modeling of reactive sputtering from an alloy target is almost as straight forward as sputtering from a single element target. Under steady-state conditions, the fraction y of one of the materials in the deposited film will be constant (identical to the target alloy composition) and independent of the value of the reactive gas supply. It should be understood, however, that, due to differences in reactivity with the reactive gas, the different metals in the alloy target may end up with quite different compound fractions θ_{c1} and θ_{c2} in the deposited film.

It should also be pointed out that, during processing, the surface composition of the alloy target normally will deviate from the target bulk composition. The fact that the overall composition of the sputter-eroded material must correspond to the target bulk composition makes it quite easy to determine the target surface concentration. The relationship between the bulk and surface composition may be found from the condition that the rate of sputtered atom emission from material 1 divided by the rate of emission from material 2 must be equal to the target bulk composition. A detailed description of modelling of reactive alloy sputtering may be found in Ref. [16].

7. Processing with several reactive gases

Sometimes, it may be desirable to form an alloy such as an oxy-nitride by reactive sputtering from a metallic

target with more than one reactive gas. The basic model may easily be modified to define a set of equations describing such a process. We assume in the following example a process having a single element metallic target sputtered in argon and two reactive gases (e.g., oxygen and nitrogen). A schematic diagram of the target conditions is shown in Fig. 24. Two reactive gases (gas 1 and gas 2) act on the target surface forming compound 1 at surface fraction θ_{t1} and compound 2 at surface fraction θ_{t2}.

There will be two balance equations defining the target steady-state condition. Analogous to Eq. (2), the balance for gas 1 and compound 1 will be:

$$\frac{J}{q} Y_{c1} \theta_{t1} = \alpha_1 2 F_1 (1 - \theta_{t1} - \theta_{t2}) \qquad (10)$$

A corresponding equation may be defined for the second gas.

The treatment of the situation at the collecting surface follows the technique outlined in the previous paragraphs.

The results of the calculations show that the process response is quite complex. The two gases compete for compound formation at the target and substrate surfaces. Both gases contribute to target poisoning. The gas gettering will strongly depend on the non-poisoned fractions $(1-\theta_{t1}-\theta_{t2})$ of the target and $(1-\theta_{c1}-\theta_{c2})$ of the collecting surfaces. Increasing the supply of gas 1, Q_1, therefore directly influences the gettering of gas 2 even without altering the supply of gas 2, Q_2. This intrinsic feedback behaviour of the process makes process control difficult [17,18].

There is a unique phenomenon that can occur during reactive sputtering with two reactive gases. It is possible to enter the target poisoning mode by increasing the supply of the first gas while keeping the second gas supply constant. During certain conditions, however, it is not possible to return to the metallic (non-poisoned) mode even by decreasing the supply of the first gas to zero. The process may be "trapped" in the target poisoned mode. The metallic mode can only be reached again if the supply of the second gas is decreased markedly below its original constant value. This phenomenon further complicates reliable control of the two gas reactive sputtering process. However, the effect is predicted by
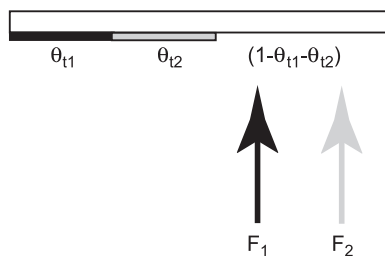

Fig. 24. Schematic of the target conditions for reactive sputtering with two reactive gases.
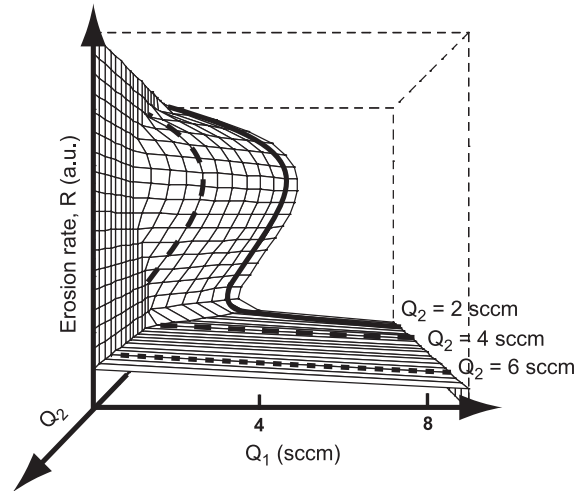

Fig. 25. Calculated sputter erosion rates, R, vs. reactive gas supplies, Q_1 and Q_2.

the results of the modelling calculations as shown in Fig. 25. The trapping effect starts to appear for approximately 4 sccm of gas 2. Once gas 1 is increased beyond the point for avalanching to the compound mode, it is not possible to return to the metallic mode even if the gas supply of gas 1 is set to zero. It is necessary to also decrease the supply of gas 2 to be able to return to the metallic mode [19,20].

8. Transient behaviour: pulsed DC reactive sputtering

During the last decade, pulsed DC reactive sputtering has become the dominating technique to power the target during reactive sputter deposition processing. This technique eliminates, or significantly reduces, the arcing problem caused by a thin insulating layer building up on the target surface. In the simulations described above, we have introduced θ_t to describe the fraction of the target consisting of compound material. If this is an insulating compound layer, it will be positively charged by the bombarding positively charged inert argon ions. A certain net charge will cause a voltage drop over the insulating layer. At a critical electrical field, an electrical breakdown of the insulating layer will take place giving rise to arcing. By changing the polarity (applying a positive voltage) from the power supply over a few percent of the duty cycle, electrons are attracted to the target surface. Proper positive voltage and duty time allow for the complete discharge of the insulating layer. In this way, arcing is prevented despite having some areas of insulating material on the target surface. The frequency of pulsed DC systems is normally in the range of 10–300 kHz.

Assuming a frequency of 100 kHz and a target erosion rate of 10 μm/min is equivalent to eroding
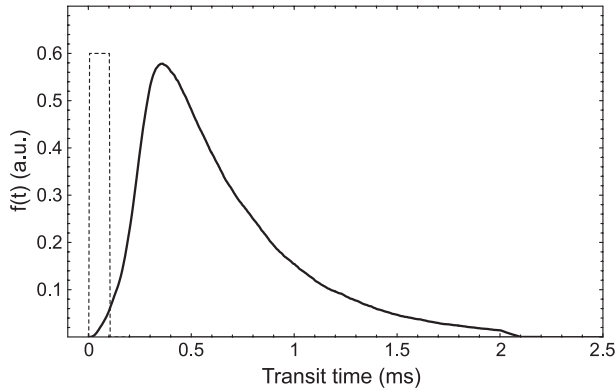
Fig. 26. Probability distribution, $f(t)$, (solid line) of the transit time for sputtered Al atoms to reach the substrate after one short (0.1 ms) sputtering pulse (dashed line).

0.0017 Å/pulse from the target surface. Such a small erosion rate per pulse is not enough to markedly change the poisoning status (θ_t) at the target. This example serves to illustrate that θ_t will not respond to the frequency of the power supply at these high frequencies. A more detailed analysis [21] shows that similar conditions will be valid for the response of θc to the applied frequency.

It should also be pointed out that there will be a transit time before sputter eroded material from the target reaches the collecting area. Due to scattering with gas atoms, there will be a dispersion in transit times for these sputtered particles. At a target to substrate distance of 10 cm and a total pressure of 5 mTorr there will be a substantial spread in transit times for sputtered Al atoms. This is illustrated in Fig. 26. The dashed short pulse (duration 0.1 ms) causes sputter erosion from an Al target. The solid curve shows the probability distribution, $f(t)$, of the transit time for sputtered atoms to reach the substrate. This result indicates that consecutive pulses from the target (frequency >1 kHz) will supply sputtered material to the collecting area with a large time overlap. The higher the frequency, the more overlap between consecutive pulses. The net result will be that the pulsed-character of arriving sputtered material will disappear. Instead, there will be a continuous flux of sputtered material as in the case of pure DC sputtering. This is illustrated in Fig. 27.

From the above arguments, we can conclude that the behaviour of the pulsed DC reactive sputtering very much will be the same as for continuous DC sputtering. The positive pulse only serves to discharge insulating parts on the target surface. The gas kinetics and flow of sputtered material will not respond fast enough to the DC pulses applied by the power supply. The short positive pulse, however, may cause some energetic bombardment at the substrate, which may influence the morphology of the deposited film. One advantage of pulsed DC operation is, however, that it allows for higher plasma densities during the "pulse on" interval as compared to the plasma density obtained for a corresponding continuous DC-plasma having the same average power.

9. Ion implantation: reactive gas

We have described some major effects that take place during reactive sputtering processes. As mentioned in the introduction we chose to include as few parameters as possible in the model, while still obtaining results which are well correlating with experimental experiences. We are aware of other effects that also take place during processing. Some of the reactive gas molecules will be ionized and gain energy from the electric field in front of the target and get implanted in the target surface region. Upon penetrating into the surface region of the target, these ions can undergo chemical reactions with the target atoms. This will cause some additional target poisoning and contribute to an increase in θ_t. In our simplified treatment, however, we assumed that the ion current is solely carried by the argon gas. This is valid when the partial pressure of the reactive gas is small compared to the partial pressure of the argon gas in the processing chamber. A detailed analysis of the effect of ion implantation of reactive gas molecules have been carried out by D. Depla and R. De Gryse. Their theoretical calculations predict that this effect alone may give rise to a hysteresis in the erosion rate vs. partial pressure curves [22]. So far, however, there exists no experimental evidence for such behaviour. The relative importance of reactive gas ion implantation and chemisorption at the target surface remains to be further investigated. Our preliminary studies indicate that the outer 20–50 Å layer at the target surface will be influenced by "knock-on" effect of energetic argon onto chemically adsorbed and/or implanted reactive gas atoms. However, irrespectively of reactive gas incorporation mechanism, the gas atoms will be evenly distributed within the whole altered target surface layer.
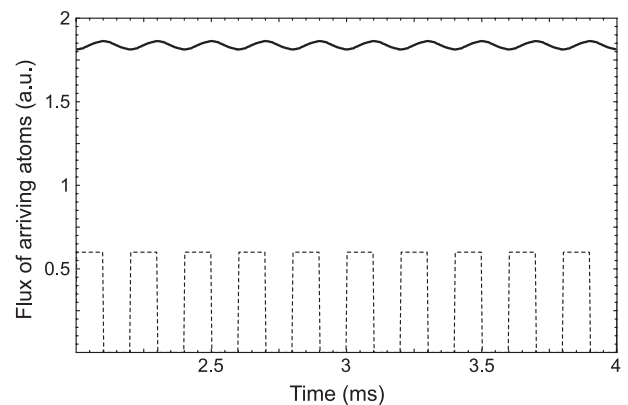

Fig. 27. Results corresponding to Fig. 26 but for a pulsed frequency of 5 kHz (dashed line).

10. Effect of secondary electrons

When the target surface composition changes, the amount of secondary electrons emitted by ion bombardment of the target surface changes. This will, in turn, change the ratio between ion and electron current. It is not possible to distinguish the electron and ion currents in the external electrical circuit. Therefore, a constant total current during processing does not necessary imply that there is a constant ion current bombarding the target. If the secondary electron emission coefficient can be estimated for the different target surface conditions, this effect can be included in the modelling work. Some authors have recently done this [23,24]. The results indicate that this effect does not change the general shapes of the calculated curves. To some extent, however, it offers a possibility to include the plasma conditions into the calculations. It is well known that the target voltage will change due to target poisoning if a reactive sputtering process operates in the constant target current mode. This can be predicted by simple calculations.

We will briefly summarize the treatment by Pflug et al. [23] who assumed that the total target current I_T is composed of both ions and electrons.

$$I_T = I(1 + \gamma), \tag{11}$$

where I denotes the actual ion current and $I\gamma$ denotes the electron current generated by the secondary emission coefficient γ. The secondary electron emission factor γ depends on both the target voltage, U, and the degree of target poisoning. Pflug et al. [23] suggested the expression

$$\gamma = (\gamma_m(1 - \theta_t) + \gamma_c\theta_t)\frac{U}{U_0} \tag{12}$$

in which γ_m and γ_c are the secondary electron emission coefficients at the metal and compound areas, respectively, at the target surface and U_0 is a reference voltage required for keeping the equation dimensionless. It is possible to combine these equations with the basic gas kinetic equations outlined in Section 2 above and calculate the variations in target voltage as a function of the reactive gas supply for constant target current. Calculated results following the treatment of Pflug et al. are shown in Fig. 28. It should be noticed that γ_m
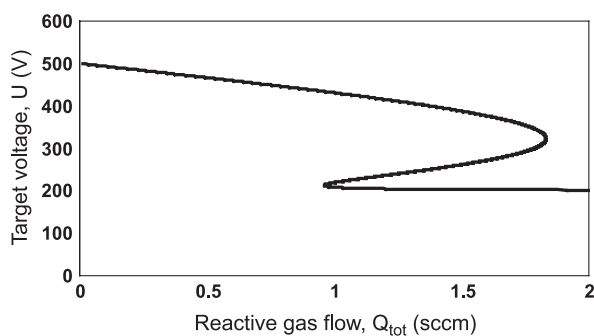
may be either smaller or larger than γ_c. Consequently, the voltage may either increase or decrease for a large supply of reactive gas. It depends on the target material and the choice of reactive gas. We may notice, however, that the processing curve is still S-shaped.

It must be pointed out, however, that the results shown in Fig. 28 are based on very simplified assumptions about the electrical characteristics of the plasma. A detailed analytical analysis can not easily be evaluated.

11. Non-uniform target current

In magnetron sputtering, the ion current is extremely non-uniform at the target. The current density in the pronounced erosion zone may be significantly higher than outside this zone. We therefore normally estimate the area of the erosion zone and assume that the current acts only on this zone. The shapes of the modeling curves, however, will not change if we assume the target to consist of different segments having different ion current densities. The degree of target poisoning, however, will be different for the different segments.

12. Modelling conclusions

The basic model presented in the first sections of this article serve to predict the general shapes of processing curves for a wide variety of reactive sputtering processes. We have also demonstrated that this model can be slightly modified quite easily to account for more complex reactive sputtering processes. It must be pointed out that the simplifications made in the model will, of course, restrict the validity of the calculated results. To our experience, however, the theoretical curves remarkable well mirror most experimental findings.

We are well aware of that much work remains to be done before there will exist a reliable detailed model which also accounts for the properties of the plasma, non-uniformities in gas kinetics, more complex chemical reactions, variations in secondary electron emission coefficients, ion implantation of the reactive gas, etc. Several attempts already exist to use finite element method (FEM) calculations to solve for some of these effects [25]. We will continue to search for new simple ways of introducing additional effects into the description of reactive sputtering processes. The basic idea is to find an extended reliable process model, which is able to predict the effects of more individual parameters.

Fig. 28. Calculated target voltage, U, as a function of the supply of the reactive gas, Q_{tot}, for reactive sputter processing at constant total target current.

Acknowledgements

Appendix A

The following parameters have been used for calculating the curves in the figures, unless otherwise is indicated.

Figs. 5–19: S=80 l/s, Y_c=0.3, Y_m=1.5, α=1, A_t=150 cm^2, A_c=2500 cm^2, I=0.5 A. Figs. 21 and 22: S=80 l/s, Y_{c1}=0.3, Y_{m1}=1.5, Y_{c2}=0.8, Y_{m2}=3.0, α_1=1, α_2=0.5, A_{t1}=150 cm^2, A_{t2}=150 cm^2, A_c=2500 cm^2, I=0.5 A. Fig. 24: S=10 l/s, Y_{c1}=0.03, Y_{m1}=0.4, Y_{c2}=0.03, Y_{m2}=0.4, α_1=1, α_2=1, A_t=18 cm^2, A_c=1650 cm^2, I=2 A. Fig. 27: P=100 W, γ_m=0.4, γ_c=1, S=80 l/s, Y_c=0.3, Y_m=1.5, α=1, A_t=150 cm^2, A_c=2500 cm^2.

References

[1] I. Safi, Surf. Coat. Technol. 127 (2000) 203.
[2] S. Berg, T. Nyberg, H.-O. Blom, C. Nender, in: D.A. Glocker, S.I. Shah (Eds.), Handbook of Thin Film Process Technology, Institute of Physics Publishing, Bristol, UK, 1998, p. A5.3:1.
[3] S. Berg, H.-O. Blom, T. Larsson, C. Nender, J. Vac. Sci. Technol., A, Vac. Surf. Films 5 (1987) 202.
[4] S. Berg, T. Larsson, C. Nender, H.-O. Blom, J. Appl. Phys. 63 (1988) 887.
[5] H. Bartzsch, P. Frach, Surf. Coat. Technol. 142/144 (2001) 192.
[6] V.A. Koss, J.L. Vossen, J. Vac. Sci. Technol., A, Vac. Surf. Films 8 (1990) 3791.
[7] H. Ofner, R. Zarwasch, E. Rille, H.K. Pulker, J. Vac. Sci. Technol., A, Vac. Surf. Films 9 (1991) 2795.
[8] H. Sekiguchi, T. Murakami, A. Kanzawa, T. Imai, T. Honda, J. Vac. Sci. Technol., A, Vac. Surf. Films 14 (1996) 2231.
[9] J.F. O'Hanlon, A User's Guide to Vacuum Technology, John Wiley & Sons, New York, NY, 1980.
[10] S. Zhu, F. Wang, W. Wu, L. Xin, C. Hu, S. Yang, S. Geng, M. Li, Y. Xiong, K. Chen, International Journal of Materials and Product Technology, Inderscience Enterprises, Guilin, China, 2001, p. 101.
[11] J. Schulte, G. Sobe, Thin Solid Films 324 (1998) 19.
[12] S. Kadlec, J. Musil, J. Vyskocil, Vacuum 37 (1987) 729.
[13] S. Berg, T. Nyberg, Patent No. WO 03/006703A1 (2001).
[14] A.J. Stirling, W.D. Westwood, Thin Solid Films 7 (1971) 1.
[15] N. Martin, C. Rousselot, Surf. Coat. Technol. 114 (1999) 235.
[16] M. Moradi, C. Nender, S. Berg, H.-O. Blom, A. Belkind, Z. Orban, J. Vac. Sci. Technol., A, Vac. Surf. Films 9 (1991) 619.
[17] W.D. Sproul, D.J. Christie, D.C. Carter, S. Berg, T. Nyberg, Proceedings of 46th Annual SVC Technical Conference, Society of Vacuum Coaters, San Francisco, CA, 2003, p. 98.
[18] N. Martin, C. Rousselot, J. Vac. Sci. Technol., A, Vac. Surf. Films 17 (1999) 2869.
[19] P. Carlsson, C. Nender, H. Barankova, S. Berg, J. Vac. Sci. Technol., A, Vac. Surf. Films 11 (1993) 1534.
[20] H. Barankova, S. Berg, P. Carlsson, C. Nender, Thin Solid Films 260 (1995) 181.
[21] L.B. Jonsson, T. Nyberg, I. Katardjiev, S. Berg, Thin Solid Films 365 (2000) 43.
[22] D. Depla, J. Haemers, R. De Gryse, Plasma Sources Sci. Technol. 11 (2002) 91.
[23] A. Pflug, B. Szyszka, V. Sittinger, J. Niemann, Proceedings of 46th Annual SVC Technical Conference, Society of Vacuum Coaters, San Francisco, CA, 2003, p. 241.
[24] Y. Matsuda, K. Otomo, H. Fujiyama, Thin Solid Films 390 (2001) 59.
[25] A. Pflug, B. Szyszka, J. Niemann, Proceedings of 4th ICCG, Braunschweig, Germany, 2002, p. 101.